

Machine learning-enabled high-entropy alloy discovery

Ziyuan Rao¹

Ye Wei^{1,2}

Po-Yen Tung¹

Ruiwen Xie³

Hongbin Zhang³

Stefan Bauer⁴

Dierk Raabe¹

Z.RAO@MPIE.DE

WEIYE@MAILS.TSINGHUA.EDU.CN

¹*Max Planck Institute for Iron Research, Duesseldorf, Germany*

²*Institute for Interdisciplinary Information Science, Tsinghua University, Peking, China*

³*Institut für Materialwissenschaft, Technische Universität Darmstadt, Darmstadt, Germany*

⁴*KTH Royal Institute of Technology; Stockholm, Sweden*

Editor: xx

Abstract

High-entropy alloys are solid solutions of multiple principal elements, capable of reaching composition and feature regimes inaccessible for dilute materials. Discovering those with valuable properties, however, relies on serendipity, as thermodynamic alloy design rules alone often fail in high-dimensional composition spaces. Here, we propose an active-learning strategy to accelerate the design of novel high-entropy Invar alloys in a practically infinite compositional space, based on very sparse data. Our approach works as a closed-loop, integrating machine learning with density-functional theory, thermodynamic calculations, and experiments. After processing and characterizing 17 new alloys (out of millions of possible compositions), we identified 2 high-entropy Invar alloys with extremely low thermal expansion coefficients around $2 \times 10^{-6} \text{ K}^{-1}$ at 300 K. Our study thus opens a new pathway for the fast and automated discovery of high-entropy alloys with optimal thermal, magnetic and electrical properties.

Keywords: Active learning; High-entropy alloys; Invar alloys;

1. Introduction

With the development of high-entropy alloys (HEAs), we have reached a new stage where multiple elements are used in similar fractions Cantor et al. (2004)Yeh et al. (2004). Considering only the most used elements of the periodic table, this spans a composition space of at least 10^{50} alloy variants, a space so large that it is impossible to tackle it by conventional alloy design methods George et al. (2019). These conventional methods for designing alloys, which have been applied to small subspaces of the HEAs composition realm, include the CALculation of PHase Diagrams (CALPHAD) and Density-Functional Theory (DFT)Mao et al. (2017)Körmann et al. (2015)Rao et al. (2019). However, CALPHAD provides equilibrium-phase diagrams only, while DFT is computationally costly and cannot be readily applied to higher temperatures and disordered alloys Körmann et al. (2015)Huang et al. (2018).

To overcome these obstacles, we propose here an active learning framework for composition discovery of HEAs, which is efficient for very sparse experimental data. The approach comprises machine learning-based techniques, density-functional theory, mean-field thermodynamic calculations, and experiments. We focus on the design of high-entropy Invar alloys with low thermal expansion coefficient (TEC), for several reasons: i) there is high demand for novel Invar alloys, for serving the huge emerging markets for the transport of liquid hydrogen, ammonia and natural gas; ii) the mechanical properties of the original $\text{Fe}_{65}\text{Ni}_{35}$ alloy for which Charles Edouard Guillaume received the 1920 physics Nobel Prize leave room for improvement; iii) alternative Invar alloys (e.g., intermetallic, amorphous or anti-ferromagnetic Invar compounds) come at forbiddingly high alloy costs and/or poor ductility Wassermann and Acet (2005) Shiga (1996); iv) although a few HEAs have the potential to fill this gap Lin et al. (2021) Rao et al. (2021), the lowest TEC ($10 \times 10^{-6} \text{ K}^{-1}$) of HEAs reported in the literature exceeds the value of the original $\text{Fe}_{65}\text{Ni}_{35}$ alloy ($1.6 \times 10^{-6} \text{ K}^{-1}$) Rao et al. (2021).

2. Methods

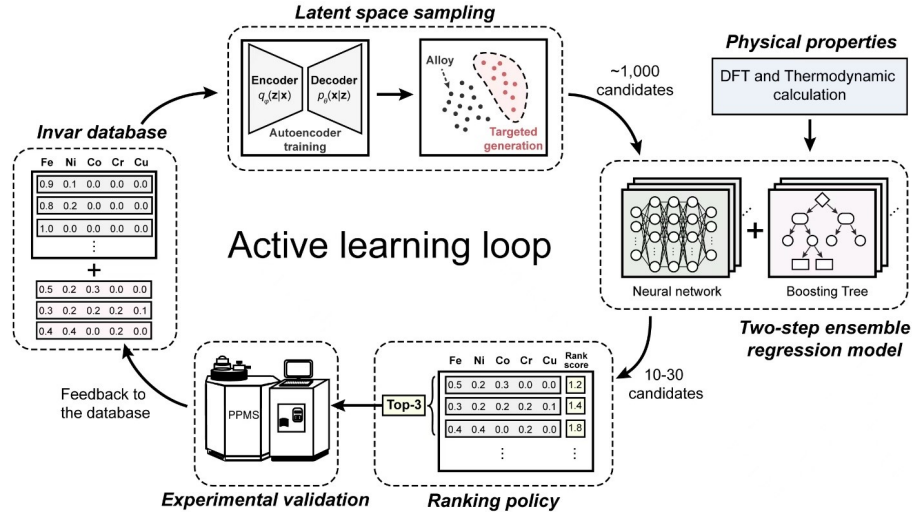


Figure 1: **Approach overview.** An active learning framework for the targeted composition design and discovery of HEAs, which combines machine learning models, DFT calculations, thermodynamic simulations and experimental feedback. Firstly, The promising candidates are generated under the HEA-GAD framework consisting of two primary steps: i) Autoencoder for composition generation. ii) Stochastic sampling for composition selection. Secondly, the selected candidates from the HEA-GAD are further processed by the TERM framework which includes two ensemble models comprised of a multilayer perceptron and gradient boosting decision tree. In the last step, the most promising compositions are selected by a ranking-based policy. The top 3 candidates are experimentally measured and fed back to the database. The iteration is repeated until the discovery of Invar alloys.

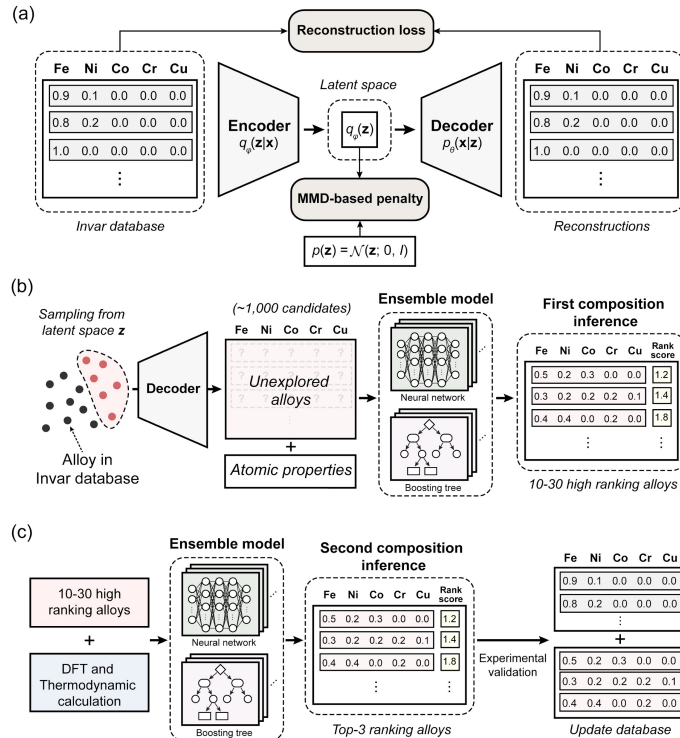


Figure 2: (a) A HEA Generative Alloy Design based on a deep generative model. The encoder takes compositions of alloys as input and the decoder can act as a generator for suggesting new alloy compositions based on the learned latent \mathbf{z} representation. (b) A large-scale screening with multilayer neural network model and gradient boosting decision tree. The new synthetic compositions with potentially low-TEC are sampled through the Markov Chain Monte Carlo method based on the latent \mathbf{z} space shown in (a). The screening utilizes the mean TEC prediction value from 100 models (including 50 multilayer perceptrons and 50 gradient boosting decision trees) as the final prediction, while the corresponding variance as the uncertainty. A rank-based objective function works as a guide to the final choice. (c) Physically informed screening model with the integration of DFT and thermodynamic calculation. The TEC of the top 3 candidates will be experimentally measured by PPMS and the results will be fed back to the training database for the next active learning iteration.

The active learning framework includes three main steps: targeted composition generation, physics-informed screening and experimental feedback (as shown in Fig. 1). In the first step, the High-Entropy Alloy Generative Alloy Design (HEA-GAD) employs a generative model (GM) to probe the 2-dimensional latent space of alloys (see Fig. 2a). GM has emerged as one of the best models for learning the latent representation of the data Ghahramani et al. (2014)Goodfellow et al. (2014). Different GMs are compared and analyzed based on the evaluation metrics. The results show that the wasserstein autoencoder (WAE) architecture performs better than other models with similar architectures, such as variational autoencoder (VAE) Tolstikhin et al. (2017)Das et al. (2021). WAE implements a typical two-neural network (NN) architecture, an encoder and a decoder. Different from VAE, WAE attempts to minimize a penalized form of the Wasserstein distance (a math-

emathical term that measures the distance between two probability distributions) between the encoded data distribution and the target distribution (see Fig. 2a). In the second step, the Two-stage Ensemble Regression Model (TERM) is used to further investigate the TEC of the HEA-GAD-generated alloy compositions (in Fig. 2b and 2c). The first stage concerns composition-based regression models, aiming at fast and large-scale composition inference. Then, the top 1,000 results with potentially low TEC from the first-stage model are screened and enter the second-stage model, where DFT and thermodynamic calculations are included as part of the input, making it a physically informed model. To increase the robustness of TERM without sacrificing the prediction accuracy, TERM taps into the advantages of MLP and GBDT by combining both into a single ensemble. The ensemble models at two stages (in Fig. 2b and 2c) adopts the same basic architecture of TERM. Such architecture consists of 50 MLPs and 50 GBDTs. Consequently, TERM utilizes the mean TEC prediction value from 100 models (including 50 MLPs and 50 GBDTs) as the final prediction, while the corresponding variance as the uncertainty of the final prediction. Finally, with a ranking strategy the TEC of the top 3 candidates is selected to be experimentally measured by PPMS (in Fig. 2c). The experimental results will augment the training database for the next active learning iteration.

3. Data Preparation

696 data points are taken from the publications Masumoto (1931)Masumoto (1934)Hakaru et al. (1954)Hakaru et al. (1955)Hakaru et al. (1957a)Hakaru et al. (1957b). 3 data points are taken from our previous unpublished work. For training, the initial dataset only occupies a very small percentage of all possible compositions. For prediction, we have 291 quaternary and 3 quinary HEAs which make the prediction even more difficult. The step size of 0.1% is considered as the resolution of the arc-melting furnace casting.

4. Results and discussion

Fig. 3a and 3b illustrate the alloy discovery process in two scenarios. In an ideal world, the composition-TEC curve is simple and convex, this means that this specific relation is readily learned and ‘never forgotten’. Even with a small dataset present, the global maxima can be easily found regardless of their initial starting points: both Path 1 and Path 2 can lead to the Invar point. However, in the real world, the lowest TEC curve is highly non-linear due to complex composition-property relations and the composition landscape remains largely unknown. Both intelligent species and algorithms will have to explore the unknown territory and accumulate knowledge about the system by making mistakes, not to mention that the composition axis is multi-dimensional, and the design space is thus huge. Therefore, the chosen Paths, available data, as well as starting points will significantly influence the final results. Path 1 may lead to local minima, while Path 2 is rather difficult initially, and multiple high TEC non-Invar can be discovered before the eventual Invar discovery. Fig. 3c and 3d provide the concentration histogram of Cr and Cu in the current dataset, respectively. We also plotted the observed lowest TEC curve to illustrate the discovery path in two HEAs. The GAD-TERM framework shows its high efficiency by quickly identifying the Invar points in the first round (A3, B2). However, the algorithm

is designed for exploration (as we discussed in the last paragraph). It inevitably discovers some non-Invar alloys along the path (e.g. A4, A8) (denoted by grey arrow). Fig. 3d clearly shows that the distribution of Cu in the alloys is extremely imbalanced, i.e., the vast majority of alloy in the dataset doesn't contain Cu at all and only a few alloys have 5% Cu. Such distributional difference likely accounts for a significantly different learning behavior observed in Fig. 3e and 3f. Fig. 4e shows the measured and predicted TEC values for FeNiCoCr and FeNiCoCrCu HEAs. Fig. 3f shows the Mean Absolute Percentage Error (MAPE) (between experiments and predictions) versus experimental iteration, with each exploitation and exploration step being marked in arrows. For FeNiCoCr HEAs, the average experimental TEC value gradually decreases: $6.49 \times 10^{-6}/\text{K}$ in the first, $5.61 \times 10^{-6}/\text{K}$ in the second and $3.65 \times 10^{-6}/\text{K}$ in the third iteration (see also Table 1). Exploration and exploitation take place alternately akin to a natural learning process, such a plot represents the 'learning curve' of the HEA-GAD-TERM model. The learning curve indicates a progressive endeavor as the MAPE error decreases significantly (from 1.5 to 0.2). In the second and third iterations, the standard deviation of the experimental TEC values declines remarkably ($3.34 \times 10^{-6}/\text{K}$ and $1.46 \times 10^{-6}/\text{K}$). This demonstrates excellent exploration progress in which HEA-GAD-TERM converges quickly and can predict TEC with high accuracy after only three iterations. On the other hand, FeNiCoCrCu shows a different learning behavior. The discovery path shows no significant improvements, from experimentally measured $6.26 \times 10^{-6}/\text{K}$ for the first iteration, to $6.64 \times 10^{-6}/\text{K}$ in the second and $5.67 \times 10^{-6}/\text{K}$ in the third iteration (more numerical details in Table 1). Such a trend can be attributed to the lack of Cu-containing FeNiCoCrCu data (only three data points are available at the beginning, see Fig. 4d). Fig. 4a shows the TEC as a function of temperatures for 2 Invar alloys ($\text{TEC} \approx 2 \times 10^{-6} \text{ K}^{-1}$) and 2 Kovar alloys ($\text{TEC} \approx 5 \times 10^{-6} \text{ K}^{-1}$) discovered in this work compared with HEAs and medium entropy alloys (MEAs) Rao et al. (2021) Laplanche et al. (2018). The alloys discovered in this work show abnormally low TEC compared to HEAs and MEAs reported before. Fig. 4b shows the configurational entropy against TEC for different kinds of alloys Schneider et al. (1995) Chanmuang et al. (2008) Fukamichi et al. (1977) Laplanche et al. (2018). Most HEAs, MEAs, and conventional alloys show high TEC values. On the contrary, most Invar alloys show a low TEC but also low configurational entropy. The Invar alloys discovered in this work offer a good combination of low TEC and high configurational entropy.

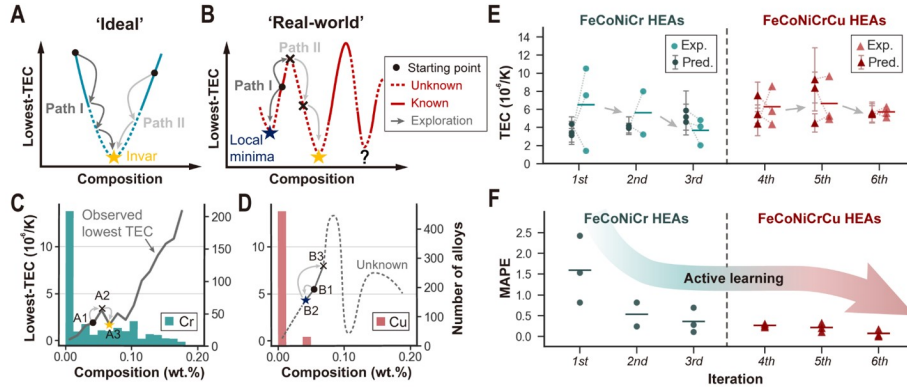


Figure 3: **Analysis of the results after 6 iterations in the active learning loop.** (a) and (b) Representation of the alloy discovery process in the ideal and real world. (c) and (d) Cr and Cu distributions histogram. The Cr histogram has various concentrations (from 0 to 20%). In contrast, the vast majority (more than 95%) of the compositions have zero Cu concentration. The lowest known TEC as a change of compositions was plotted as solid curves while the dashed curves represent the unknown. Grey arrows illustrate the discovery paths of HEA-GAD-TERM. (e) Experimental TEC of the FeNiCoCr and FeNiCoCrCu HEAs. Predictions and experimental results are marked in triangles and rectangles, respectively. (f) MAPE of active learning. Each exploitation and exploration step was marked in arrows, and the dots represent the MAPE between experiment and predictions. Alternations between exploration and exploitation are akin to a natural learning process.

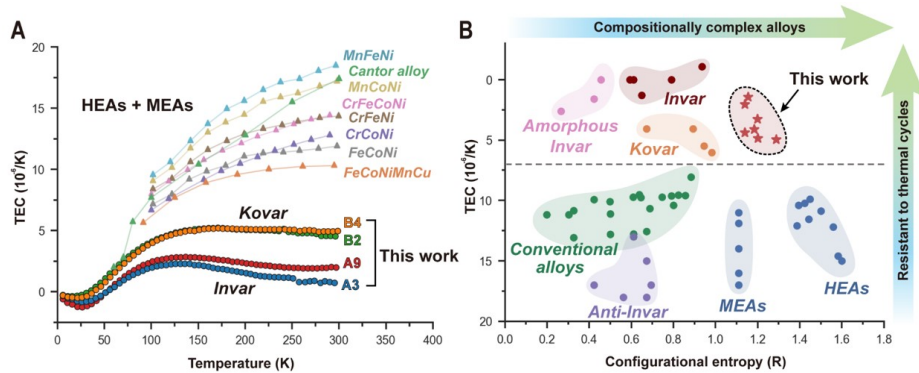


Figure 4: **A summary of the excellent properties of the ML-designed HEAs in this work.** (a) The thermal expansion coefficient of the ML-designed HEAs as a change of temperature. As a comparison, we plot the thermal expansion curve of the HEAs and MEAs. A3 and A9 FeNiCoCr HEAs show extremely low TECs around $2 \times 10^{-6} \text{ K}^{-1}$ at 300 K which can be used as Invar alloys. B2 and B4 FeNiCoCrCu HEAs show low TECs around $5 \times 10^{-6} \text{ K}^{-1}$ at 300 K which can be used as Kovar alloys. (b) Configurational entropy plotted against the TEC values for various known alloys and alloys discovered in this work. ML enables this work to efficiently discover new alloys with excellent properties (high resistance to thermal cycles) in an infinite phase spectrum (compositionally complex alloys).

Acknowledgments

We would like to acknowledge support for this project from the National Science Foundation Z.R., R.X., O.G. and H.Z. appreciate the funding by Deutsche Forschungsgemeinschaft (DFG, German Research Foundation) - Project-ID 405553726 – TRR 270. Y.W. appreciates the funding by BiGmax, the Max Planck Society’s Research Network on Big-Data-Driven Materials Science and acknowledges the financial support from the ERC-CoG-SHINE-771602. P.T. acknowledges the financial support by Electron and X-ray microscopy Community for structural and chemical Imaging Techniques for Earth materials (EXCITE) - grant number G106564 and International Max Planck Research School for Interface Controlled Materials for Energy Conservation (IMPRS-SurMat). The contributions of Prof. M. Acet, M. Nellessen, M. Adamek and F. Schlüter are also gratefully acknowledged. The Lichtenberg high-performance computer of TU Darmstadt is gratefully acknowledged for providing computational resources for the EMTO calculations in the present work.

References

- Brain Cantor, ITH Chang, Peter Knight, and AJB Vincent. Microstructural development in equiatomic multicomponent alloys. *Materials Science and Engineering: A*, 375:213–218, 2004.
- C Chanmuang, M Naksata, T Chairuangstri, H Jain, and CE Lyman. Microscopy and strength of borosilicate glass-to-kovar alloy joints. *Materials Science and Engineering: A*, 474(1-2):218–224, 2008.
- Payel Das, Tom Sercu, Kahini Wadhawan, Inkit Padhi, Sebastian Gehrman, Flaviu Cipci-gan, Vijil Chenthamarakshan, Hendrik Strobelt, Cicero Dos Santos, Pin-Yu Chen, et al. Accelerated antimicrobial discovery via deep generative models and molecular dynamics simulations. *Nature Biomedical Engineering*, 5(6):613–623, 2021.
- K Fukamichi, M Kikuchi, S Arakawa, and T Masumoto. Invar-type new ferromagnetic amorphous fe-b alloys. *Solid State Communications*, 23(12):955–958, 1977.
- Easo P George, Dierk Raabe, and Robert O Ritchie. High-entropy alloys. *Nature reviews materials*, 4(8):515–534, 2019.
- In Z Ghahramani, M Welling, C Cortes, ND Lawrence, and KQ Weinberger. Transportability from multiple environments with limited experiments: Completeness results. 2014.
- Ian Goodfellow, Jean Pouget-Abadie, Mehdi Mirza, Bing Xu, David Warde-Farley, Sherjil Ozair, Aaron Courville, and Yoshua Bengio. Generative adversarial nets. *Advances in neural information processing systems*, 27, 2014.
- MASUMOTO Hakaru, SAITO Hideo, and KONO Tatsuo. Influence of addition of nickel on the thermal expansion, rigidity modulus and its temperature coefficient of the alloys of cobalt, iron and chromium, especially of co-elinvar. i: Additions of 10 and 20 per cent of nickel. . *A , = Science reports of the Research Institutes, Tohoku University. Ser. A, Physics, chemistry and metallurgy*, (6):529–538, 1954.

- MASUMOTO Hakaru, SAITO Hideo, and SUGAI Yutaka. Influence of addition of nickel on the thermal expansion, rigidity modulus and its temperature coefficient of the alloys of cobalt, iron and chromium, especially of co-elinvar. ii: Additions of 30 and 40 per cent of nickel. . *A , = Science reports of the Research Institutes, Tohoku University. Ser. A, Physics, chemistry and metallurgy*, (7):533–540, 1955.
- MASUMOTO Hakaru, SAITO Hideo, and GOTO Kimiyosi. Influence of addition of nickel on the thermal expansion, the rigidity modulus and its temperature coefficient of the alloys of cobalt, iron and vanadium. . *A , = Science reports of the Research Institutes, Tohoku University. Ser. A, Physics, chemistry and metallurgy*, (9):159–169, 1957a.
- MASUMOTO Hakaru, SAITO Hideo, and SUGAI Yutaka. Influence of addition of copper on the characteristics of an elinvar type alloy” co-elinvar”. i: Alloys containing 5 per cent of copper. . *A , = Science reports of the Research Institutes, Tohoku University. Ser. A, Physics, chemistry and metallurgy*, (9):170–175, 1957b.
- Shuo Huang, Erik Holmström, Olle Eriksson, and Levente Vitos. Mapping the magnetic transition temperatures for medium-and high-entropy alloys. *Intermetallics*, 95:80–84, 2018.
- Fritz Körmann, Duancheng Ma, Dustin D Belyea, Matthew S Lucas, Casey W Miller, Blazej Grabowski, and Marcel HF Sluiter. “treasure maps” for magnetic high-entropy-alloys from theory and experiment. *Applied Physics Letters*, 107(14):142404, 2015.
- G Laplanche, P Gadaud, C Bärsch, K Demtröder, C Reinhart, J Schreuer, and EP George. Elastic moduli and thermal expansion coefficients of medium-entropy subsystems of the crmnfeconi high-entropy alloy. *Journal of Alloys and Compounds*, 746:244–255, 2018.
- Chun-Lin Lin, Tso-Wei Chen, Yao-Jen Chang, Hideyuki Murakami, Seiji Mitani, and An-Chou Yeh. Dimensional stability of a metastable fcc high entropy alloy. *Applied Physics Letters*, 119(17):171902, 2021.
- Huahai Mao, Hai-Lin Chen, and Qing Chen. Tchea1: A thermodynamic database not limited for “high entropy” alloys. *Journal of Phase Equilibria and Diffusion*, 38(4):353–368, 2017.
- H Masumoto. On the thermal expansion of the alloys of iron, nickel, and cobalt and the cause of the small expansibility of alloys of the invar type. *Science Reports of the Tohoku Imperial University*, 20:101–123, 1931.
- H Masumoto. On the thermal expansion of alloys of cobalt, iron, and chromium, and a new alloy, “stainless-invar”. *Sci. Report. Tohoku. Imp. Univ*, 23(2):265–275, 1934.
- Ziyuan Rao, Dirk Ponge, Fritz Körmann, Yuji Ikeda, Oldřich Schneeweiss, Martin Friák, Jörg Neugebauer, Dierk Raabe, and Zhiming Li. Invar effects in fenico medium entropy alloys: From an invar treasure map to alloy design. *Intermetallics*, 111:106520, 2019.
- Ziyuan Rao, Aslı Çakır, Özge Özgün, Dirk Ponge, Dierk Raabe, Zhiming Li, and Mehmet Acet. 3 d transition-metal high-entropy invar alloy developed by adjusting the valence-electron concentration. *Physical Review Materials*, 5(4):044406, 2021.

- T Schneider, M Acet, B Rellinghaus, EF Wassermann, and W Pepperhoff. Antiferromagnetic invar and anti-invar in fe-mn alloys. *Physical Review B*, 51(14):8917, 1995.
- Masayuki Shiga. Invar alloys. *Current Opinion in Solid State and Materials Science*, 1(3):340–348, 1996.
- Ilya Tolstikhin, Olivier Bousquet, Sylvain Gelly, and Bernhard Schoelkopf. Wasserstein auto-encoders. *arXiv preprint arXiv:1711.01558*, 2017.
- EF Wassermann and M Acet. Invar and anti-invar: magnetovolume effects in fe-based alloys revisited. In *Magnetism and Structure in Functional Materials*, pages 177–197. Springer, 2005.
- J-W Yeh, S-K Chen, S-J Lin, J-Y Gan, T-S Chin, T-T Shun, C-H Tsau, and S-Y Chang. Nanostructured high-entropy alloys with multiple principal elements: novel alloy design concepts and outcomes. *Advanced engineering materials*, 6(5):299–303, 2004.